MIMO Radar Antenna with Sectorial Human Torso Illumination for an In-Cabin Breathing Detection System

María-José López*, César Palacios*, Jordi Romeu*, Luis Jofre-Roca*
*Dept. Signal Theory and Communications, Technical University of Catalonia, Barcelona, Spain
corresponding author: maria.jose.lopez.montero@upc.edu

***Abstract*—The vital sign measurement systems inside vehicles have taken great or impulse in recent years, and the technologies that have been most welcomed are based on wireless measurements that do not interrupt driving and are imperceptible to the driver. There are disorders in breathing patterns, which include the movement of different regions of the human thorax mainly. In this sense, the objective of this paper is to determine the dimensions of a lens-based antenna system and the pointing angles of the radiation main lobe of the six antenna-elements to measure the elongation of six regions of the human torso and determine breathing patterns. The pointing angle is controlled by the position of the antenna behind the lens, and the beamwidth of the lobe depends on the directivity achieved by the antenna. An electronic system to simulate torso elongation is also presented to calibrate and test the sensitivity of the system.**

***Index Terms*—antennas, electromagnetics, propagation, measurements.**

I. Introduction

In recent years, many efforts have been devoted to the development of vital signal control systems within vehicles that seek to meet two essential characteristics: they should not be intrusive while driving and they should be sensitive enough. The detection and measurement of breathing rate has been studied using contact [1]–[4] and non-contact [5]–[9] systems, both in indoor and outdoor environments. Within closed environments there are also investigations that deal with the detection of vital signs inside vehicles [10]–[12] . Wireless based systems has been well received for In-Cabin monitoring.

Breathing pattern disorders are patterns of over or under breathing, where depth and breathing are excessive or insufficient to the needs of the body, they are usually erratic and are detectable after a long period of time. Several of these patterns include movement of the thoracic and abdominal parts, and may be caused by anxiety problems, drowsiness, tiredness, cardiovascular problems, etc. [13]. Torso elongation due to breathing pattern disorders may be synchronized or paradoxical, and also asymetrical between the left and right side. As presented in literature, when a person performs the breathing process some section of the torso moves up to about 30.0 mm [14]–[16] in some cases. This displacement cause a time delay in the received signal that is prone to be measured using appropriate antenna systems [17]–[19]. The space inside the vehicle is limited, for this reason, to determine the ideal monitoring conditions, an optimal beamwidth and lens size are of fundamental importance, since it directly provides a correct illumination for torso regions elongation measurement.

This paper is the first phase of the development of a system to measure the elongation of six torso regions in order to identify breathing pattern disorders in a driver or passenger of a vehicle. This first phase consists of presenting a system of antennas capable of pointing and covering each of the six regions and measuring their elongation. The study is focused on controlling the pointing angle and beamwidth of the radiation pattern of six radar antennas.

Therefore, the objectives of this work are: (i) to deploy a brief state-of-the-art on breathing pattern disorders measurements; (ii) to develop a system of antennas to aim and adequately cover six regions of the human torso; and (iii) to present a torso movement emulator system for calibration and sensitivity measurements. Theoretical analysis and numerical simulations have been conducted to determine the optimal lens dimensions and position that provides the proper pointing and focusing angles of the radiation pattern.

The paper has been organized as follows: Section I shows the introduction of the work. Section II presents the theoretical background for the determination of the lens dimensions and the variance of the pointing angle with respect to the antenna position behind the lens. Section III shows the methods and systems used. Section IV focuses on presenting results, and Section V closes the work with the conclusions.

II. Theoretical background

In a FMCW radar, the incident chirp is a sinusoidal signal with amplitude A_t ant initial phase Φ^{inc} along the time t, represented as $s^{inc}(t) = A_t \exp\left(j(2\pi f_c t + \pi \frac{BW}{T_s} t^2 + \Phi^{inc}(t))\right)$, whit a carrier frequency f_c, a bandwidth BW, and a period T_s that is linearly swept in the range $f_c \pm BW/2$. The positive or negative displacement $d_{ts}(t)$ of each torso region during breathing, causes a delay $t^{del} = \frac{2(r^i_{at}(\theta,\phi)+d_t s(t))}{c}$ on the transmitted signal, where r^i_{at} is the initial distance between the antenna and the respective region i, and the factor of 2 represents the round-trip time of the reflected wave. Fig.1 depicts the and artist-view of the scenario. The beat signal produced by the product of the incident and reflected signal [17]–[21], can be written as:

$$s^{IF}(t) = A \exp(j(4\pi \frac{BW}{T_s} \frac{r^i_{at}}{c} t + \Phi(t))) \qquad (1)$$

http://dx.doi.org/10.23919/EuCAP57121.2023.10133775

where,

$$\Phi(t) = 4\pi \frac{r_{at}^{i}}{\lambda} \tag{2}$$

represents the phase change caused by torso motion. Finally, by applying the Fast Fourier Transform (FFT), frequency value in the x-axis is proportional to the target distance, and the peak value corresponds to the power of the received signal.Then, by applying an algorithm for finding peak-maximum along the time, the breathing signal can be determined.

To detect abnormal breathing patterns during driving, six regions of the torso have been defined as follows: from the clavicle to the height of the armpit (4Rib) the left and right upper thoracic (LUTh, RUTh) regions; then, from the armpit (4Rib) to the (9Rib), the left-right lower thoracic (LLTh, RLTh) regions, has been defined; and, in the abdominal section of the torso the left-right abdominal (LHAb, RHAb) regions.

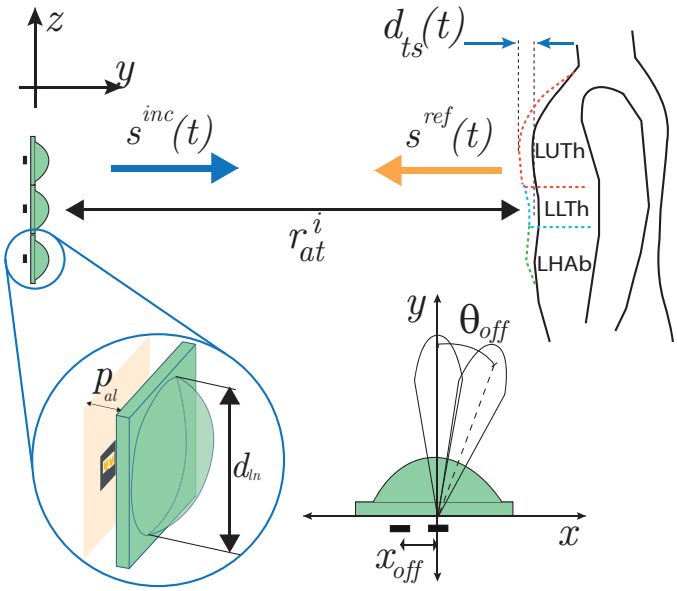

Fig. 1: Artist-view of the proposed scenario. The diagram shows only the Left side regions of the human torso.

When a lens is placed in front of an antenna, the radiation pattern becomes focused and directivity increases [22]. Using the geometry of Fig. 1, the regions on the torso has been initially defined to be $10.0\,\mathrm{cm} \times 10.0\,\mathrm{cm}$, so for each one of them, an equation is defined to estimate the lens diameter from the directivity of the antenna, to cover effectively the surface of a single region.

The calculation of the antenna directivity depends on the integration of the power pattern over a spherical surface, which results in a complex computation. In most practical cases, simpler expressions can be used for approximate and fast calculations according to the lobe shape. For antennas with a narrow major lobe, the directivity D_{ln} after the lens can be estimated using the approximation of Cardama [22] as,

$$D_{ln} = \frac{4\pi}{\Delta\theta^{E}_{-3\,\mathrm{dB}} \Delta\theta^{H}_{-3\,\mathrm{dB}}} = \frac{4\pi (r_{at}^{i})^{2}}{l_{ot} w_{ot}} \tag{3}$$

where $\Delta\theta^{E}_{-3\,\mathrm{dB}}$ and $\Delta\theta^{H}_{-3\,\mathrm{dB}}$ are the half power bandwidth (HPBW) of two orthogonal planes, r_{at}^{i} is the distance between the antenna and the region, and $\mathrm{l}_{o}t$ and w_{ot}, are the width and height of the sinlge region. The effective area of the lens with a diameter d_{ln} can be expressed as;

$$A_{ef}^{ln} \approx 0.8 A_{ln} \approx 0.8\pi \left(\frac{d_{ln}}{2}\right)^{2}, \tag{4}$$

and the directivity in terms of the effective area would be,

$$D_{ln} = \frac{4\pi A_{ef}^{ln}}{\lambda^{2}} \tag{5}$$

where λ is the wavelength at the frequency of operation. After that, by clearing the equation to find the lens diameter, it is equal to

$$d_{ln} = 1.25 \frac{\lambda r_{at}^{i}}{\sqrt{l_{ot} w_{ot}\,(0.5\pi)}} \tag{6}$$

The position of the antenna behind the lens determines the pointing angle at which the radiation lobe reaches the torso. Eventually, the distance p_{al} between the antenna and the lens may adjust its final beamwidth. As shown in the lower right of Fig. 1, a longitudinal variation (x-axis) or transverse (y-axis) of the antenna corresponds to a variation in the pointing angle in two orthogonal planes of the radiation lobe. The scan angles θ^{E}_{scn} and θ^{H}_{scn}, defined as the angle variation in the E-plane and H-plane, respectively, has been estimated in terms of the antenna displacement, as

$$\theta^{E}_{scn} \cong \frac{x_{off} \Delta\theta^{E}_{-3\,\mathrm{dB}}}{\lambda/2}, \tag{7}$$

and

$$\theta^{H}_{scn} \cong \frac{y_{off} \Delta\theta^{H}_{-3\,\mathrm{dB}}}{\lambda/2}. \tag{8}$$

III. Methods and System Description

This section describes the elements of the system and presents the methods applied to meet the objectives of the paper. This study has been developed in two parts. The first part consists on to deploy numerical simulations to estimate the spot generated from the beamwidth of the radiation pattern of the antennas when reach the torso region. And, the second part of the study focuses on the construction of a torso elongation emulator phantom that allows probing the necessary signal sensitivity and spatial resolution on the antennas that enables torso elongation measurements.

A. Radar Antenna system

Chest and abdominal movements were measured with a commercial experimental radar operating at the 122 GHz ISM band with a 6 GHz frequency bandwidth, a noise figure of 8.7 dB, and based on a set of four microstrip patch antennas for each one of the beams, resulting into a range resolution of 10.0 m. The radar front-end (RFE) uses chirp signal with a frequency-modulated continuous-wave (FMCW). The received data is packaged in the form of frames, that are transmitted by

a serial communication bus to a host computer to be analyzed and plotted using Matlab. The antennas are placed in a 3x2 array, each pointing to the respective torso region. The distance between the torso and the radars is $65.0\,\mathrm{cm}$. To measure the elongation of each region, a spectrogram is constructed from the instantaneous elongation measured over slow time, as shown in Fig. 2a. Then, by applying an algorithm for finding peak-maximum, the breathing signal can be extracted from the spectrum, as show in Fig. 2b. The breathing exercise consisted of 10 seconds of breathing simulation at 20 breath/min then 20 seconds of apnea and continue at the same rate until complete 60 seconds.

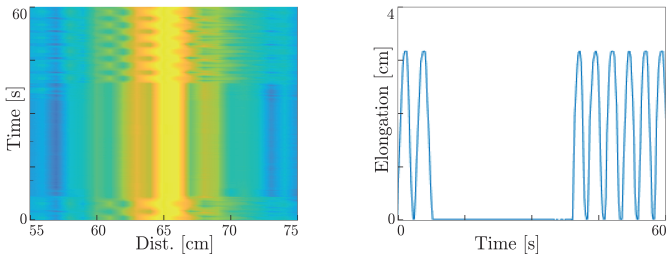

(a) (b)

Fig. 2: Breathing detection spectrum (a) and time signal (b). Both plots correspond to the same breathing exercise.

B. Dielectric lens description

A dielectric lens of polylactic acid (PLA) with a relative dielectric permittivity $\varepsilon_{ln} = 3.1$ has been placed at $p_{al} = 15.0\,\mathrm{mm}$ from the chip antennas, to enhance directivity and reach the desired beamwidth. The lens system consists of a square base plate of $w_{bp} = 36.0\,\mathrm{mm}$ on which a $30.0\,\mathrm{mm}$-diameter lens d_{ln} has been situated. The overall thickness of the lens is $15.7\,\mathrm{mm}$. To aim each of the regions the pointing angle is controlled according to the position of the antenna behind the lenses. The distance to the target is $65.0\,\mathrm{cm}$, and by default the antenna is pointing the Xiphoid process between the upper and lower thoracic regions. As depicted in Fig. 3.

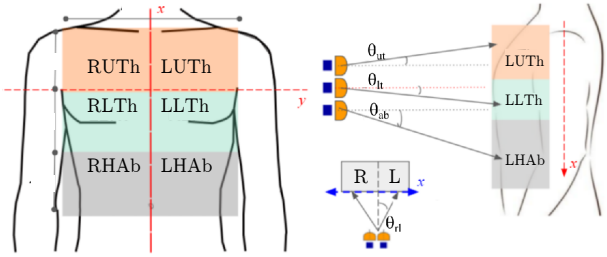

Fig. 3: Size of elongation modes and defocus angle for each region

C. Simulation process

The beamwidth of the antennas has been simulated, in terms of its longitudinal and transversal resolution, in order to reconstruct the elliptical spot. The simulations are carried out by using comprehensive electromagnetic simulation software, FEKO which uses the MoMFEM (method of moment/finite element method). In order to compute the size of the spot, the length of the major and minor radius of the ellipse must be calculated. The antenna has been designed and simulated along with the dielectric lens, which transforms the HPBW at $-3\,\mathrm{dB}$ from 46.8^o to 6.4^o. The human torso is simulated using a plate of $10.0\,\mathrm{cm} \times 10.0\,\mathrm{cm}$ with a layer of skin-like ($\varepsilon_{sk} = 5.6$, $\sigma_{sk} = 39,4\ S/m$), and muscle-like ($\varepsilon_{ms} = 8.6, \sigma_{ms} = 62.5\ S/m$) [23], located at a distance of 65.0 cm from the lens, as depict in Fig. 4.

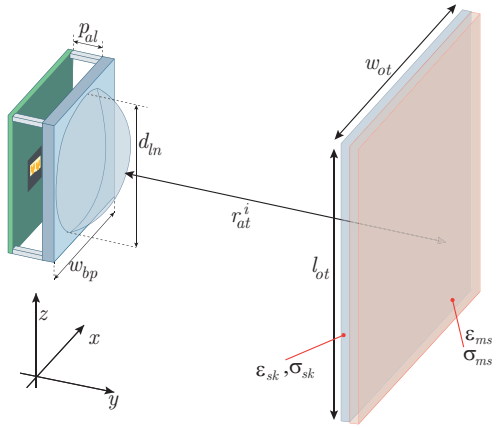

Fig. 4: Equivalent system for elongation modes measurements

D. Breathing simulator phantom

Because testing breathing pattern disorders on one person would involve long days of experimentation that would be too strenuous, to test the system an emulator of torso elongation has been designed and fabricated. The phantom is based on a mechanical system that displaces plates of real relative permittivity similar to that of the skin, ε_{sk}. To fine-vary the pointing angle, the antennas, as shown in Fig. 5, have been mounted on two-axis positioners, which allow them to be moved both horizontally and vertically.

The movement of each of the engines is commanded by a microcontroller, which has been programmed with the elongation information of each individual region according to breathing patterns.

IV. Results

The lens in front of the antennas improves the directivity of the antenna by $30\,\mathrm{dB}$, the results of the half power beam width (HPBW) are shown in Fig. 6. Considering, the geometry shown in Fig. 4, with $r_{at} = 65.0\,\mathrm{cm}$, the height l_{ot} and the width w_{ot} of the single region equal to $10.0\,\mathrm{cm}$, and $\lambda = 2.4 \times^{-3}\,\mathrm{m}$; the estimated diameter of the lens should be around $d_{ln} = 3.0\,\mathrm{cm}$. Acording to equation 6, a commercial lens of diameter 3.0cm has been used for focusing. An individual antenna behind the lens has been moved transversally and longitudinally, for pointing in the E- and H- planes. As show the Fig. 3, the upper thoracic region is reached by moving the

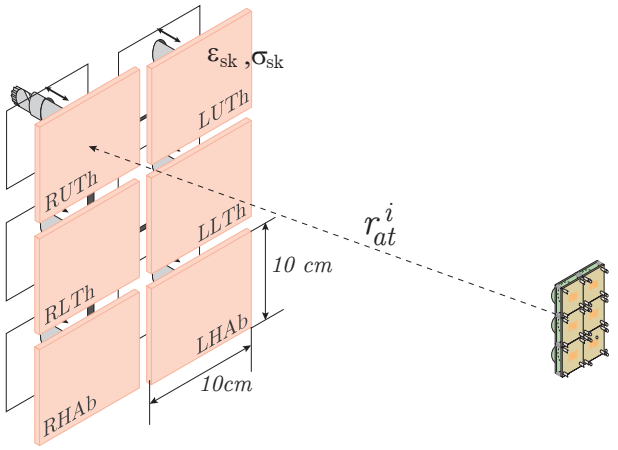

Fig. 5: The mechanical part of the simulator is controlled with DC motors, and the position of the antennas is varied with optomechanical parts.

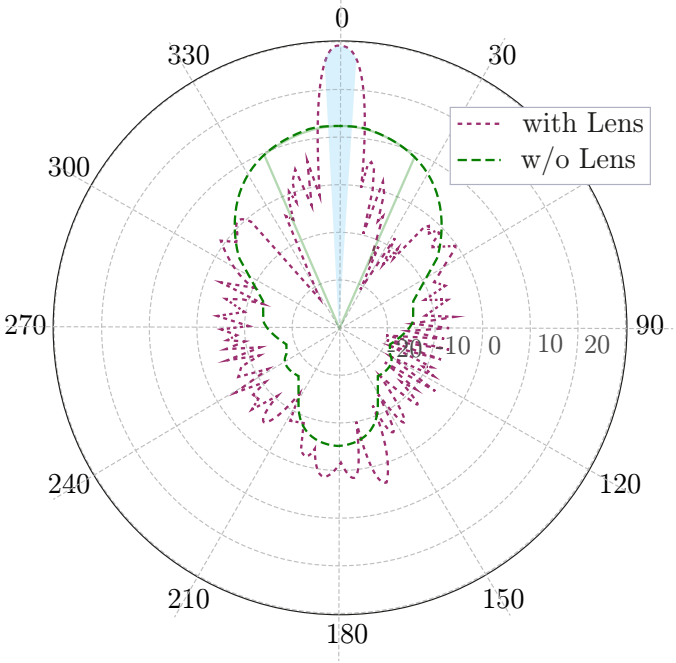

Fig. 6: HPBW without lens is 46.8^o and with lens 6.4^o degrees.

antenna $\lambda_{fs}/2$ in the negative x-axis direction, that is an angle θ_{ut}=2.1^o; for the lower thoracic region the pointing angle is θ_{lt}=-2.3^o and the antenna was displaced $\lambda_{fs}/2$ in the positive x-axis direction; and for the abdominal region, θ_{ab}=5.4^o, and the antenna position is λ_{fs} in the positive x-axis from the center. In the H-plane the left and right sides have been reached by moving antennas 3/2λ_{fs} in the negative and positive y-axis to form an angle of θ_{rl}=8.2^o from the center of the torso.

Once the aiming angles have been defined, it is necessary to perform a simulation and an experimental estimation of the spot created by each radiation lobe. To reconstruct the major and minor axes of the elliptic spot footprint to illuminate each of the regions, the HPWB at -3 dB of the beam in the E- and H-planes has been used. Using Matlab the ellipse is reconstructed, as plotted in Fig. 7, for each of the regions, the average effective covered area of the six antenna radars is 50%. The beamwidth for each region and the size of the spot has been summarized on table I.

Region	HPBW H-Plane (^{o})	HPBW E-Plane (^{o})	Minor axis (cm)	Major axis (cm)
LUTh	5.4	5.8	6.7	6.2
RUTh	6.5	5.8	6.7	7.3
LLTh	6.3	5.9	6.7	7.2
RLTh	7.4	5.9	6.7	8.4
LA	11.8	6.1	6.9	13.4
RA	11.5	6.1	6.9	13.4

TABLE I: Beamwidth angles from FEKO and computed minor and major diameter of the spot using Matlab

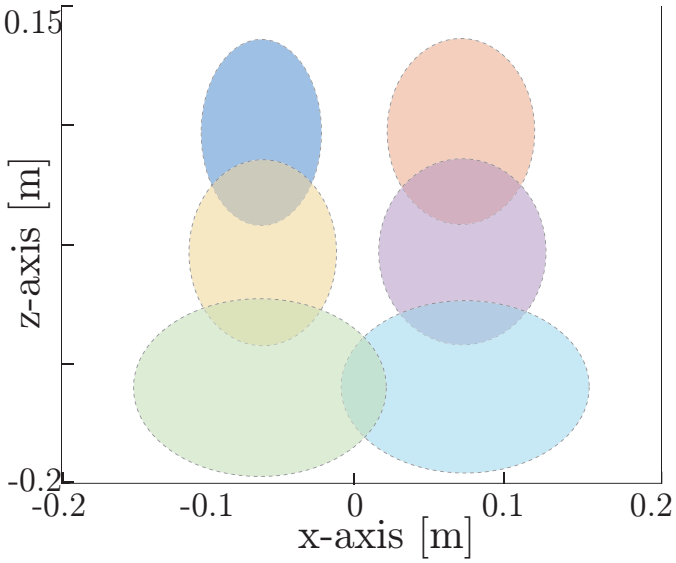

Fig. 7: Each region corresponds to one of the elongation modes.

To verify the aim and focus of each antenna, an experiment was carried out that consisted of putting the six radars into operation and activating each of the regions of the elongation simulator individually. Then the signal from the six radars was measured in order to determine the added noise in the deactivated regions. The measured breathing rate for six different time periods where only one region was active at once is shown in Fig. 8.

V. Conclusions

An antenna system capable of accurately wirelesly illuminating six individual regions of the human torso has been analyzed. Pointing to each of the regions is controlled by varying the position of the antennas behind a lens. And the focus is calculated from the effective illuminated area according to the beamwidth of the radiation lobe in the E and H plane.

The displacement of the antennas to get the proper pointing angles is of the order of a few λ units, while the lens is 120

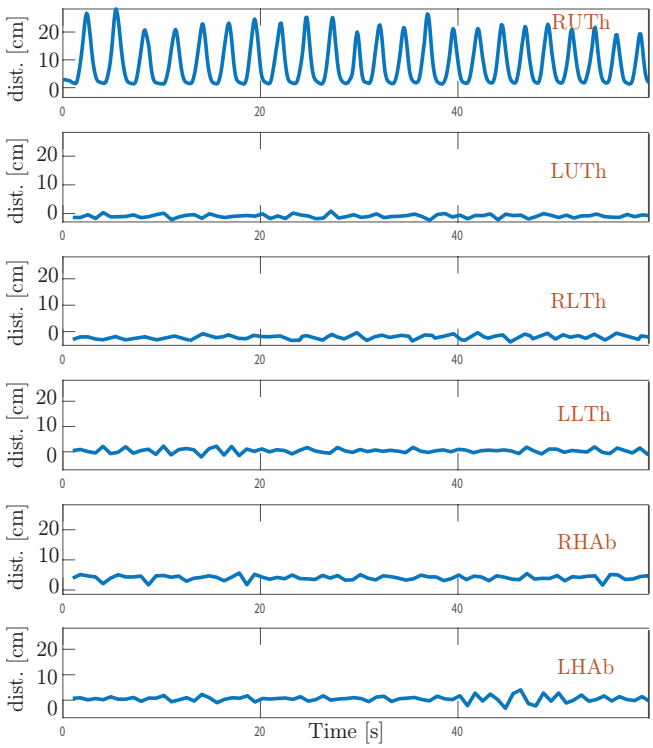

Fig. 8: The Upper thoracic region has been activated in the elongation simulator meanwhile the others are immobile.

times larger. This means that all six antennas could eventually be placed on the same lens.

Acknowledgment

This work was supported by the Spanish "Comision Interministerial de Ciencia y Tecnologia" (CICYT) under projects PID2019-107885GB-C31 and MDM2016-O6OO; Catalan Research Group 2017 SGR 219; and "Secretaría Nacional de Educación Superior, Ciencia, Tecnología e Innovación" (SENESCYT) from the Ecuadorian government.

References

[1] G. Tomich, D. França, A. Diório, R. Britto, R. Sampaio, and V. Parreira, "Breathing pattern, thoracoabdominal motion and muscular activity during three breathing exercises," *Brazilian Journal of Medical and Biological Research*, vol. 40, no. 10, pp. 1409–1417, 2007.

[2] V. F. Parreira, C. J. Bueno, D. C. França, D. S. Vieira, D. R. Pereira, and R. R. Britto, "Breathing pattern and thoracoabdominal motion in healthy individuals: influence of age and sex," *Brazilian Journal of Physical Therapy*, vol. 14, pp. 411–416, 2010.

[3] M. Weenk, H. van Goor, B. Frietman, L. J. Engelen, C. J. van Laarhoven, J. Smit, S. J. Bredie, and T. H. van de Belt, "Continuous monitoring of vital signs using wearable devices on the general ward: pilot study," *JMIR mHealth and uHealth*, vol. 5, no. 7, p. e91, 2017.

[4] A. M. Chan, N. Selvaraj, N. Ferdosi, and R. Narasimhan, "Wireless patch sensor for remote monitoring of heart rate, respiration, activity, and falls," in *2013 35th Annual international conference of the IEEE engineering in medicine and biology society (EMBC)*. IEEE, 2013, pp. 6115–6118.

[5] A. Prat, S. Blanch, A. Aguasca, J. Romeu, and A. Broquetas, "Collimated beam fmcw radar for vital sign patient monitoring," *IEEE Transactions on Antennas and Propagation*, vol. 67, no. 8, pp. 5073–5080, 2018.

[6] K. Yamamoto, K. Toyoda, and T. Ohtsuki, "Cnn-based respiration rate estimation in indoor environments via mimo fmcw radar," in *2019 IEEE Global Communications Conference (GLOBECOM)*. IEEE, 2019, pp. 1–6.

[7] M. Sidikova, R. Martinek, A. Kawala-Sterniuk, M. Ladrova, R. Jaros, L. Danys, and P. Simonik, "Vital sign monitoring in car seats based on electrocardiography, ballistocardiography and seismocardiography: A review," *Sensors*, vol. 20, no. 19, p. 5699, 2020.

[8] E. Turppa, J. M. Kortelainen, O. Antropov, and T. Kiuru, "Vital sign monitoring using fmcw radar in various sleeping scenarios," *Sensors*, vol. 20, no. 22, p. 6505, 2020.

[9] M. Alizadeh, G. Shaker, J. C. M. De Almeida, P. P. Morita, and S. Safavi-Naeini, "Remote monitoring of human vital signs using mm-wave fmcw radar," *IEEE Access*, vol. 7, pp. 54 958–54 968, 2019.

[10] I. Nejadgholi, H. Sadreazami, Z. Baird, S. Rajan, and M. Bolic, "Estimation of breathing rate with confidence interval using single-channel cw radar," *Journal of healthcare engineering*, vol. 2019, 2019.

[11] K. Van Loon, M. Breteler, L. Van Wolfwinkel, A. R. Leyssius, S. Kossen, C. Kalkman, B. van Zaane, and L. Peelen, "Wireless non-invasive continuous respiratory monitoring with fmcw radar: a clinical validation study," *Journal of clinical monitoring and computing*, vol. 30, no. 6, pp. 797–805, 2016.

[12] A. Lazaro, M. Lazaro, R. Villarino, and D. Girbau, "Seat-occupancy detection system and breathing rate monitoring based on a low-cost mm-wave radar at 60 ghz," *IEEE Access*, vol. 9, pp. 115 403–115 414, 2021.

[13] E. Denton, J. Bondarenko, and M. Hew, "Breathing pattern disorder," *Complex Breathlessness (ERS Monograph). Sheffield, European Respiratory Society*, pp. 109–122, 2022.

[14] M. Ragnarsdóttir and E. K. Kristinsdóttir, "Breathing movements and breathing patterns among healthy men and women 20–69 years of age," *Respiration*, vol. 73, no. 1, pp. 48–54, 2006.

[15] H. Kaneko and J. Horie, "Breathing movements of the chest and abdominal wall in healthy subjects," *Respiratory care*, vol. 57, no. 9, pp. 1442–1451, 2012.

[16] T. Kondo, I. Kobayashi, Y. Taguchi, Y. Ohta, and N. Yanagimachi, "A dynamic analysis of chest wall motions with mri in healthy young subjects *," *Respirology*, vol. 5, no. 1, pp. 19–25, 2000. [Online]. Available: https://onlinelibrary.wiley.com/doi/abs/10.1046/j.1440-1843.2000.00221.x

[17] H. Lee, B.-H. Kim, J.-K. Park, S. W. Kim, and J.-G. Yook, "A resolution enhancement technique for remote monitoring of the vital signs of multiple subjects using a 24 ghz bandwidth-limited fmcw radar," *IEEE Access*, vol. 8, pp. 1240–1248, 2019.

[18] L. Anitori, A. de Jong, and F. Nennie, "Fmcw radar for life-sign detection," in *2009 IEEE Radar Conference*. IEEE, 2009, pp. 1–6.

[19] M. He, Y. Nian, and Y. Gong, "Novel signal processing method for vital sign monitoring using fmcw radar," *Biomedical Signal Processing and Control*, vol. 33, pp. 335–345, 2017.

[20] A. Anghel, G. Vasile, R. Cacoveanu, C. Ioana, and S. Ciochina, "Short-range wideband fmcw radar for millimetric displacement measurements," *IEEE Transactions on Geoscience and Remote Sensing*, vol. 52, no. 9, pp. 5633–5642, 2014.

[21] G. Wang, J.-M. Munoz-Ferreras, C. Gu, C. Li, and R. Gomez-Garcia, "Application of linear-frequency-modulated continuous-wave (lfmcw) radars for tracking of vital signs," *IEEE transactions on microwave theory and techniques*, vol. 62, no. 6, pp. 1387–1399, 2014.

[22] Á. C. Aznar, J. R. Robert, J. M. R. Casals, L. J. Roca, S. B. Boris, and M. F. Bataller, *Antenas*. Univ. Politèc. de Catalunya, 2004.

[23] A. Christ, A. Aeschbacher, F. Rouholahnejad, T. Samaras, B. Tarigan, and N. Kuster, "Reflection properties of the human skin from 40 to 110 ghz: A confirmation study," *Bioelectromagnetics*, vol. 42, no. 7, pp. 562–574, 2021.